

Cite this: *Dalton Trans.*, 2019, **48**, 17741

Enhanced Heck reaction on flower-like Co(Mg or Ni)Al layered double hydroxide supported ultrafine PdCo alloy nanocluster catalysts: the promotional effect of Co[†]

Jin Li, Ying Song, Yajuan Wang and Hui Zhang *

A series of PdCo alloy nanocluster (NC) catalysts x -PdCo _{r} /Co(Mg or Ni)Al-LDH (x : Pd loading, r : Co/Pd molar ratio) were synthesized by immobilizing ultrafine PdCo _{r} -PVP NCs on flower-like layered double hydroxide (LDH) supports. The sizes of PdCo alloy NCs of the catalysts can be elaborately tuned in ~1.6–3.2 nm by both Co/Pd ratios and Pd loadings, and the PdCo NCs are mainly dispersed on the edge sites of LDH nanosheets upon a flower-like morphology. The PdCo bimetallic catalysts 0.81-PdCo_{0.10}/MgAl-LDH (2.6 ± 0.6 nm), 0.86-PdCo_{0.28}/MgAl-LDH (2.3 ± 0.7 nm) and 0.79-PdCo_{0.54}/MgAl-LDH (3.2 ± 0.9 nm) exhibit enhanced activity compared with the monometallic Pd catalyst for Heck coupling of iodobenzene with styrene. Particularly, 0.86-PdCo_{0.28}/MgAl-LDH shows the highest activity, which can be attributed to its smallest PdCo_{0.28} alloy NCs, and the maximum electron density of the Pd⁰ center resulted from the electron transfer from Co and the strongest PdCo_{0.28} NCs – LDH synergistic effect. 0.67-PdCo_{0.28}/CoAl-LDH shows much better activity than those of 0.64-PdCo_{0.28}/NiAl-LDH and 0.86-PdCo_{0.28}/MgAl-LDH. The lowest Pd loading sample 0.01-PdCo_{0.28}/CoAl-LDH (1.6 ± 0.4 nm) shows an ultrahigh turnover frequency of 163 000 h⁻¹ (Pd: 1.9 × 10⁻⁵ mol%), which is the highest value obtained so far. Meanwhile, the catalyst shows excellent adaptability for the substrates and can be reused for 12 runs without significant loss of activity. The present work may provide a new idea for the simple and green synthesis of ultrafine Pd-based non-noble bimetallic catalysts for varied catalytic processes.

Received 12th September 2019,
Accepted 5th November 2019

DOI: 10.1039/c9dt03663f

rsc.li/dalton

Introduction

The palladium-catalyzed Heck reaction is one of the most important paths for constructing C–C bonds with one step^{1,2} and has been widely used for synthesizing natural products,³ pharmaceuticals,⁴ and fine chemicals.⁵ However, conventional homogeneous Pd-based catalysts such as Pd(PPh₃)₄ and PdCl₂(PPh₃)₂,⁶ Pd-carbene complexes⁷ and cyclic Pd compounds⁸ often suffer from the difficulty of separation and recovery, easily lost activity and environmental pollution. Therefore, heterogeneous Pd-based catalysts by supporting Pd or Pd–M alloy nanoparticles (NPs) on varied supports such as polymers,^{9,10} carbon or silica-based materials,^{11,12} metal oxides,¹³ and hydroxalates^{14,15} have become a research hotspot in recent years.

Considering the consumption of expensive Pd, the introduction of non-noble metal elements such as Ni,^{16,17} Cu¹⁸ and Co^{19–21} can not only reduce costs, but also stabilize active Pd species, and the obtained Pd-based bimetallic catalysts can exhibit greatly improved C–C coupling reactivity due to the adjustable geometry and electronic structure involving the electron transfer, coordination environment, lattice strain and distribution of surface elements. Bai *et al.*¹⁶ prepared carbon nanofiber (CNF)-loaded Pd–Ni catalysts by electrospinning, then by ethylene glycol reduction, followed by high-temperature carbonization for Suzuki coupling of aryl halide with phenylboronic acid, of which Pd₁Ni₄/CNF (~4 nm) gave the highest biphenyl yield of 96.55%. Shaabani *et al.*¹⁹ reported PdCo ANP-PPI-*g*-graphene (2–3 nm) *via* the co-complexation of PdCl₂ and CoCl₂·6H₂O precursors with PPI-grafted-graphene followed by NaBH₄ reduction for Sonogashira reaction of iodobenzene with phenylacetylene, producing a diphenylacetylene yield of 99%, which was much higher than the monometallic ones. However, the preparation of the above-mentioned supports, CNF and PPI-*g*-graphene hybrid, suffers from tedious and time-consuming processes, and the size of bimetallic NPs is relatively larger, which greatly limits further improvement of the activity of these catalysts.

State Key Laboratory of Chemical Resource Engineering, Beijing University of Chemical Technology, P.O. Box 98, Beijing 100029, China.

E-mail: huizhang67@gst21.com, zhanghui@mail.buct.edu.cn; Fax: +86 10 64425385; Tel: +86 10 64425872

[†]Electronic supplementary information (ESI) available. See DOI: 10.1039/C9DT03663F

Layered double hydroxides (LDHs), which are typical anionic clay materials, possess controllable morphology, large surface area, highly ordered and tunable layer elements, and intrinsic alkalinity along with easy preparation, and thus they are widely used as catalysts or supports.²² Choudary *et al.*¹⁴ prepared a plate-like MgAl-LDH-supported Pd catalyst LDH-Pd⁰ (4–6 nm) through an ion exchange of PdCl₄²⁻ with the interlayer Cl⁻ ions of LDH followed by hydrazine hydrate reduction for Heck olefination of 4-chloroanisole with styrene, and the catalyst exhibited superior activity to those of other supported Pd catalysts. Wu *et al.*²³ reported simple plate-like MgAl-LDH-loaded Au-Pd alloy NPs by using the impregnation–reduction step for the selective photocatalytic oxidation of benzyl alcohol, and Au₁-Pd₉/LDH (~4.2 nm) showed the highest conversion rate of 91.1%, which was much higher than those of its monometallic counterparts. Li *et al.*²⁴ prepared flower-like Au/NiAl-LDH catalysts (2.24–2.99 nm) *via* sol immobilization of Au-PVA NPs on NiAl-LDH for the selective oxidation of benzyl alcohol, and the catalysts showed higher activity than that of the common plate-like Au/NiAl-LDH, which could be attributed to the confinement effect of hierarchical pores improving the effective collisions between substrates and active sites. However, to the best of our knowledge, there are no reports about hierarchical flower-like LDH supported ultrafine Pd-based non-noble bimetallic catalysts so far, and therefore it is highly desirable that these catalysts are fabricated and used for the efficient Heck reaction.

Herein, a series of flower-like PdCo alloy nanocluster (NC) catalysts *x*-PdCo_{*r*}/Co(Mg or Ni)Al-LDH (*x*: Pd loading, *r*: Co/Pd molar ratio) were fabricated *via* an ethylene glycol reduction–sol immobilization method for Heck reaction. The Co/Pd ratios, Pd loadings and elemental compositions of LDH in the obtained catalysts have a significant effect on Heck reactivity, and 0.01-PdCo_{0.28}/CoAl-LDH exhibits an ultrahigh turnover frequency of 163 000 h⁻¹. Moreover, the catalyst shows excellent adaptability for the substrates and recyclability. Combined with systematic characterization results and kinetic analysis, a possible mechanism of the Heck reaction over the present catalysts was tentatively proposed.

Experimental section

Materials and chemicals

Poly(*N*-vinyl-2-pyrrolidone) (PVP, k-30) was purchased from Xilong Chemical Corporation. Cobalt chloride hexahydrate (CoCl₂·6H₂O), ethylene glycol (EG), *N,N*-dimethylformamide (DMF), K₂CO₃, and KCl were bought from Beijing Chemical Works. Palladium chloride (PdCl₂), styrene and bromobenzene were purchased from Tianjin Fuchen Chemicals Reagent Factory. Iodobenzene and other aryl halides were purchased from Aladdin. All chemicals were of analytical grade and used without further purification. The deionized water with a resistivity >18.25 MΩ cm (25 °C) was used in all experiments.

The synthesis of flower-like Co(Mg or Ni)Al-LDH supports

Flower-like Co(Mg or Ni)Al-LDH supports were prepared by a simple constant-pH coprecipitation method.²⁵ Typically, 100 mL of alkaline solution containing 0.800 g of NaOH and 0.636 g of Na₂CO₃ was added dropwise into 100 mL of deionized water under vigorous stirring until the pH reached 10 ± 0.1 and was kept for 5 min. Then another 100 mL of aqueous solution containing 9 mmol Co(NO₃)₂·6H₂O (or Mg(NO₃)₂·6H₂O or Ni(NO₃)₂·6H₂O) and 3 mmol Al(NO₃)₃·9H₂O was added dropwise into the above solution by keeping a pH of 10 ± 0.1 by simultaneously adding alkaline solution under vigorous stirring. The resulting slurry was aged at 65 °C for 4 h, cooled to room temperature (25 °C) and washed with deionized water until the pH was ~7, and finally the obtained precipitate was dried at 60 °C for 24 h, giving flower-like Co (Mg or Ni)Al-LDH supports.

The synthesis of PdCo_{*r*}-PVP alloy nanoclusters (NCs)

The PdCo_{*r*}-PVP colloidal NCs were prepared by a modified polyol reduction method.²⁶ Firstly, 1.000 g of PdCl₂ (5.64 mmol) and 0.843 g of KCl (11.3 mmol) were totally dissolved in 100 mL of deionized water, resulting in a K₂PdCl₄ solution (0.056 mol L⁻¹). 1.190 g of CoCl₂·6H₂O (5 mmol) was totally dissolved in 100 mL of deionized water, resulting in a CoCl₂ solution (0.050 mol L⁻¹). A certain amount of PVP upon (Co + Pd)/PVP = 10/1 (mol/mol), 2.5 mL of K₂PdCl₄ solution and a certain amount of CoCl₂ solution (Co/Pd molar ratio designed as 0.1, 0.3 or 0.6) were added into 150 mL of deionized water, followed by adding 50 mL of EG. Then, a NaOH solution (1 mol L⁻¹) was added to adjust the pH to ~12; the mixture was refluxed at 140 °C in an oil bath for 2 h and then cooled to room temperature, obtaining the dark-brown colloidal solution named PdCo_{*r*}-PVP NCs. For comparison, monometallic Pd-PVP or Co-PVP NCs were prepared by following similar steps using K₂PdCl₄ solution or CoCl₂ solution as the precursor.

The synthesis of flower-like PdCo alloy NC catalysts *x*-PdCo_{*r*}/Co(Mg or Ni)Al-LDH

Flower-like catalysts *x*-PdCo_{*r*}/Co(Mg or Ni)Al-LDH were prepared by a sol immobilization method. Typically, 1.500 g of flower-like MgAl-LDH support was added into 200 mL of the above-mentioned PdCo_{*r*}-PVP colloidal solution upon a theoretical Pd loading of 1.0 wt% under vigorous stirring for 2 h at room temperature. The resultants were centrifuged and washed three times with acetone and deionized water alternately, and finally dried at 60 °C overnight to obtain a powdery product designated as *x*-PdCo_{*r*}/MgAl-LDH (*r*: Co/Pd ratio of 0.10, 0.28 and 0.54; *x*: Pd loading in wt%; ICP). For comparison, flower-like monometallic Pd/MgAl-LDH (Pd: 0.80 wt%, ICP) and Co/MgAl-LDH (Co: 0.85 wt%, ICP) were prepared by a similar method. By replacing MgAl-LDH support with CoAl-LDH and NiAl-LDH, flower-like catalysts 0.67-PdCo_{0.28}/CoAl-LDH and 0.64-PdCo_{0.28}/NiAl-LDH were obtained, respectively. Reduced Pd loading samples



Scheme 1 The design schematic of flower-like catalysts $x\text{-PdCo}_r/\text{Co}(\text{Mg or Ni})\text{Al-LDH}$.

0.10- $\text{PdCo}_{0.28}/\text{CoAl-LDH}$ and 0.01- $\text{PdCo}_{0.28}/\text{CoAl-LDH}$ were obtained by reducing the usage of the $\text{PdCo}_r\text{-PVP}$ NC colloidal solution to 100 mL and 20 mL, respectively. Scheme 1 depicts the design schematic of the flower-like $x\text{-PdCo}_r/\text{Co}(\text{Mg or Ni})\text{Al-LDH}$ catalysts.

Characterization

The X-ray diffraction (XRD) analysis of the samples was carried out using a Shimadzu XRD-6000 X-ray powder diffractometer equipped with $\text{Cu K}\alpha$ radiation (1.5418 Å, 40 kV, 30 mA). The $\text{PdCo}_r\text{-PVP}$ NC colloidal solution was dried at 80 °C in a vacuum for 24 h and ground into the powder for the XRD test. The FT-IR spectra were recorded with a Bruker Vector-22 FT-IR spectrophotometer using the KBr pellet technique (sample/KBr = 1/100). The surface morphology of the samples was analyzed by using a Zeiss supra 55 Scanning electron microscope (SEM), and the surface elements and contents were detected by the DXGENSIS60 energy scattering spectrometer. High resolution transmission electron microscopy (HRTEM) was performed by using a JEM 2010 high resolution transmission electron microscope. High-angle annular dark-field scanning transmission electron microscopy (HAADF-STEM) with energy-dispersive X-ray spectroscopy was performed using a JEOL JEM-2100F transmission electron microscope. The contents of Pd, Co, Ni, Mg and Al in the samples were analyzed using the Shimadzu ICPS-7500 inductively coupled plasma atomic emission spectrometer (ICP-AES). The surface electronic structure and composition of the samples were analyzed using a VG-ESCALAB 250 X-ray photoelectron spectrometer (XPS) at a base pressure in the analysis chamber of 2×10^{-9} Pa using a standard Al $\text{K}\alpha$ source (1486.6 eV). The binding energy was referenced to the C 1s line of surface contamination carbon C 1s (284.9 eV). CO adsorption *in situ* FT-IR spectra were recorded on a Nicolet 380 instrument containing a controlled environment chamber equipped with CaF_2 windows. 30 mg of samples were compressed into tablets and fixed in a ceramic sample chamber. Prior to testing, the samples were kept for 1 h in N_2 flow (50 mL min^{-1}) and scanned to obtain a background spectrum. Then it was exposed into CO flow (50 mL min^{-1}) for 1 h, and finally purged with N_2 (50 mL min^{-1}) for 0.5 h. The IR spectrum was recorded in absorbance mode with a resolution of 4 cm^{-1} .

Activity test

The Heck reaction was carried out using a 25 mL three-necked round-bottom flask attached to a reflux condenser under magnetic stirring. Aryl halide (1.0 mmol), alkene (1.5 mmol), K_2CO_3 (3 mmol), catalyst (an appropriate amount of Pd with respect to aryl halide), DMF (12 mL) and H_2O (4 mL) were mixed in the flask, and then the reaction was allowed to proceed at 120 °C under magnetic stirring at atmospheric pressure. The products were analyzed by using the Agilent 7890A gas chromatograph equipped with an Agilent J&K HP-5 capillary column (5% phenyl polysiloxane, $30 \text{ m} \times 0.25 \text{ mm} \times 0.25 \mu\text{m}$) and a flame ionization detector for quantitative analysis using the peak area normalized method. After reaction, the catalyst was separated by centrifugation and thoroughly washed 4 times with DMF and water for the next run. The filtrate was extracted by ethyl acetate to obtain an organic phase which was dried by adding anhydrous Na_2SO_4 , followed by rotary evaporation (45 °C) to remove the solvent, and then recrystallized to obtain the products for ^1H and ^{13}C NMR analysis (see the ESI†).

Results and discussion

The ultrafine bimetallic $\text{PdCo}_r\text{-PVP}$ NCs were first synthesized by ethylene glycol reduction at 140 °C, and their XRD patterns are shown in Fig. 1A. Clearly, with increasing Co/Pd ratios, three $\text{PdCo}_r\text{-PVP}$ NCs ($r = 0.10, 0.28$ and 0.54 by ICP) show gradually upshifted diffraction peaks at 2θ ca. $40.60^\circ, 41.13^\circ$ and 41.59° indexed to a reduced $d_{(111)}$ of 0.222, 0.219 and 0.217 nm, respectively, all between 0.225 nm of Pd-PVP (the same as *fcc* Pd of JCPDS 46-1043) and 0.205 nm of Co-PVP NCs (the same as *fcc* Co of JCPDS 15-0806), implying the formation of the PdCo_r alloy phase, which is consistent with Vegard's law.²⁷ These gradually reduced $d_{(111)}$ values can be ascribed to the lattice contraction of Pd due to the incorporation of Co into the Pd *fcc* structure.^{28–30} The HRTEM images in Fig. 1B and C reveal the average size of $\text{PdCo}_{0.28}\text{-PVP}$ NCs as $1.5 \pm 0.5 \text{ nm}$, and the (111) plane lattice fringes with spacings of 0.220 nm, further confirming the formation of the alloy state of ultrafine $\text{PdCo}_{0.28}$ NCs.

Then a series of PdCo alloy NC catalysts $x\text{-PdCo}_r/\text{Co}(\text{Mg or Ni})\text{Al-LDH}$ ($x = 0.01\text{--}0.86 \text{ wt\%}$ by ICP) were fabricated by sup-

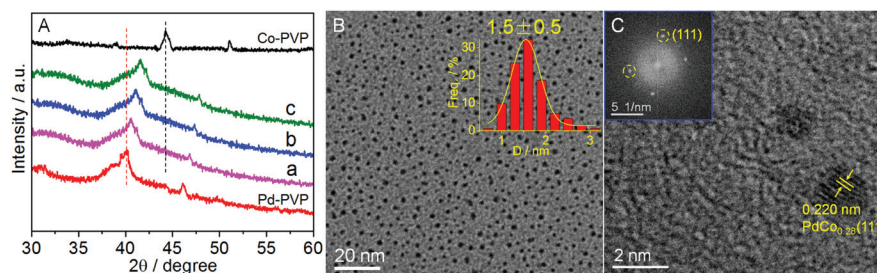


Fig. 1 XRD patterns (A) of PdCo_r-PVP ($r = 0.10$ (a), 0.28 (b) and 0.54 (c)) NCs compared with Pd-PVP and Co-PVP NCs, and HRTEM images (B and C) of PdCo_{0.28}-PVP NCs (insets: histogram of particle size distribution and fast Fourier transform image (FFT)).

porting PdCo_r-PVP NCs on flower-like Co(Mg or Ni)Al-LDH supports *via* the sol immobilization method (Scheme 1), and their XRD patterns are shown in Fig. 2. All the catalysts show quite similar diffractions to their supports except for a slightly weakened peak intensity at 2θ ca. 11.5° , 23.2° , 34.9° , 39.6° , 46.8° , 60.6° and 61.8° indexed to the (003), (006), (012), (015), (018), (110) and (113) planes of typical hexagonal LDH phase,^{25,31} respectively. The sharp and strong (003) peaks with d_{003} in 0.754 – 0.766 nm (Table S1†) indicate the presence of the CO₃²⁻-LDH phase.³¹ It can be seen from Table S1† that x -PdCo_r/MgAl-LDH possesses a larger D_{110} (~ 58 nm) and D_{003} (~ 14.5 nm) than those of 0.64 -PdCo_{0.28}/NiAl-LDH (25.4 nm, 11.5 nm) and x -PdCo_{0.28}/CoAl-LDH (~ 49.8 nm, ~ 14.7 nm), probably due to the combinational effect of the electronegativity and cation radii of different LDH layer metals. It is noteworthy that no characteristic diffraction peaks related to

PdCo alloy NCs are observed, implying the ultrafine size and high dispersion of PdCo alloy NCs in the as-obtained catalysts.

The FT-IR spectra (Fig. S1†) of a series of flower-like PdCo alloy NC catalysts x -PdCo_r/Co(Mg or Ni)Al-LDH compared with monometallic catalysts and their corresponding supports as well as PVP show broad and strong absorptions at ~ 3500 cm⁻¹ due to the stretching vibration of -OH groups of the LDH laminate or physically adsorbed water molecules.³¹ The PVP shows wide peaks in 2950 – 2850 cm⁻¹ due to the ν (symmetric stretching) mode of CH₃ or CH₂, a strong peak at 1680 cm⁻¹ due to the ν (-C=O) mode, and sharp peaks at 1290 cm⁻¹ due to the ν (-CN) mode.³² For all the catalysts and supports, sharp peaks at 1370 cm⁻¹ and weak ones at 860 cm⁻¹ can be assigned to the ν_3 and ν_2 (out-of-plane deformation) modes of CO₃²⁻ anions, respectively, and sharp peaks at 665 and 420 cm⁻¹ can be attributed to the lattice vibration of the Co(Ni, Mg and Al)-O bond and the Co(Ni, Mg and Al)-OH bond in the LDH laminates,³² respectively, further confirming the existence of the CO₃²⁻-LDH phase. It is to be noted that, the blueshift of the bending vibration of the LDH interlayer water to ~ 1655 cm⁻¹ compared to supports (1640 cm⁻¹) and obvious broaden band in 2950 – 2850 cm⁻¹ from ν (-CH₃/CH₂) of PVP, imply the possible interaction between PdCo_r NCs and LDH supports *via* hydrogen bonds between tertiary amino groups or carbonyl groups of PVP in PVP-protected PdCo_r alloy NCs and hydroxyl groups on the LDH laminates causing the change of the chemical environment of water molecules in LDH interlayer.

The SEM images of 0.86 -PdCo_{0.28}/MgAl-LDH, 0.64 -PdCo_{0.28}/NiAl-LDH and 0.67 -PdCo_{0.28}/CoAl-LDH (Fig. S2a-c†) clearly show flower-like structures, quite similar to the corresponding supports (Fig. S2a₀-c₀†), assembled from staggered LDH nanosheets with sizes of ~ 196 , 186 , and 210 nm and thicknesses of ~ 17.0 , 11.1 and 14.0 nm, respectively, implying approximately a side by side arrangement of ~ 4 , 8 , 4 primary LDH nanoplates upon Scherrer dimensions (Table S1†). The corresponding EDS spectra (Fig. S2a'-c'†) clearly show the existence of Pd and Co elements besides Mg (or Ni or Co), Al, C and O signals.

The HRTEM images of 0.81 -PdCo_{0.10}/MgAl-LDH, 0.86 -PdCo_{0.28}/MgAl-LDH and 0.79 -PdCo_{0.54}/MgAl-LDH (Fig. 3a₁-a₃) show the sizes of PdCo NCs of 2.6 ± 0.6 , 2.3 ± 0.7 , and 3.2 ± 0.9 nm, respectively, between Pd/MgAl-LDH (2.0 ± 0.8 nm, Fig. S3a†) and Co/MgAl-LDH (4.8 ± 1.2 nm, Fig. S3b†), indicat-

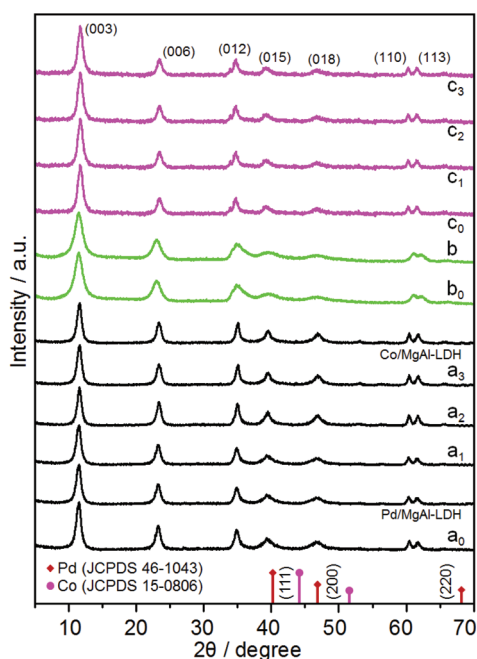


Fig. 2 XRD patterns of the 0.81 -PdCo_{0.10}/MgAl-LDH (a₁), 0.86 -PdCo_{0.28}/MgAl-LDH (a₂), 0.79 -PdCo_{0.54}/MgAl-LDH (a₃), 0.64 -PdCo_{0.28}/NiAl-LDH (b), x -PdCo_{0.28}/CoAl-LDH ($x = 0.67$ (c₁), 0.10 (c₂), 0.01 (c₃)) compared with Pd/MgAl-LDH, Co/MgAl-LDH and related supports (a₀-c₀).

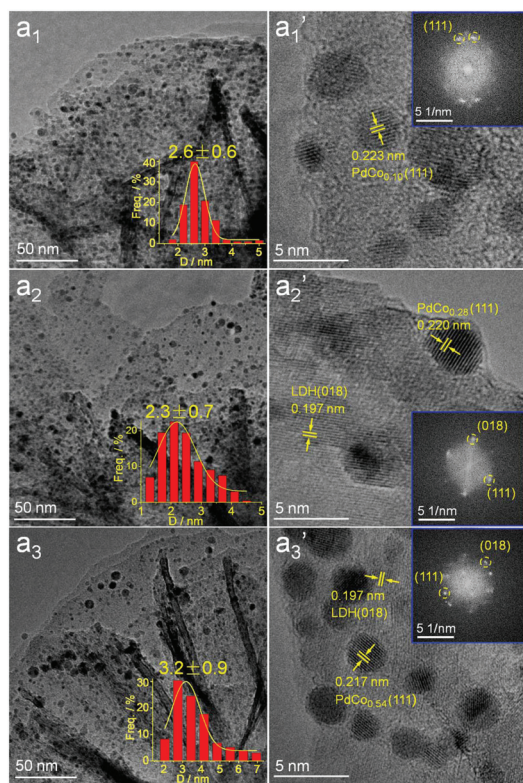


Fig. 3 HRTEM images of 0.81-PdCo_{0.10}/MgAl-LDH (a₁, a₁'), 0.86-PdCo_{0.28}/MgAl-LDH (a₂, a₂') and 0.79-PdCo_{0.54}/MgAl-LDH (a₃, a₃') (insets: particle size distribution and FFT).

ing that the sizes of PdCo alloy NCs can be effectively tuned by Co/Pd ratios in obtained catalysts. The high-magnified HRTEM images (Fig. 3a₁'–a₃') show the lattice fringe spacings of the PdCo NCs (111) plane of 0.223, 0.220 and 0.217 nm, respectively, between Pd/MgAl-LDH (0.225 nm, Fig. S3a†) and Co/MgAl-LDH (0.205 nm, Fig. S3b†), further indicating the formation of the PdCo alloy phase. Meanwhile, lattice fringes with spacings of 0.197 nm are also observed in three samples, indexed to the hexagonal LDH (018) plane. It is noteworthy that the PdCo alloy NCs are predominantly anchored on the edge sites of LDH nanosheets, suggesting the possible existence of strong interaction between PdCo alloy NCs and LDH nanosheets in the catalysts.^{33,34}

The HADDF-STEM-EDX line scanning analysis (Fig. 4) of 0.81-PdCo_{0.10}/MgAl-LDH, 0.86-PdCo_{0.28}/MgAl-LDH and 0.79-PdCo_{0.54}/MgAl-LDH (selecting larger NCs to meet the detection limit of the device) reveals the presence of both Pd and Co signals at the same position, confirming the formation of the PdCo alloy phase and gradually enhanced Co signals with increasing Co/Pd ratio. The HADDF-STEM image (Fig. S4a†) of 0.86-PdCo_{0.28}/MgAl-LDH shows the average size of PdCo_{0.28} alloy NCs of 2.2 ± 0.6 nm, and the mapping results show the almost overlapped Pd and Co signals besides the evenly dispersed Mg and Al elements, further demonstrating the alloy state of PdCo NCs. The EDX (Fig. S4b†) spectrum shows a Co/Pd ratio of 0.29, in line with ICP result.

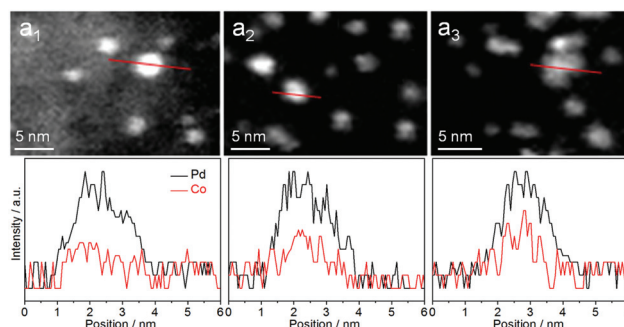


Fig. 4 HADDF-STEM images and the corresponding EDX line scanning profiles of 0.81-PdCo_{0.10}/MgAl-LDH (a₁), 0.86-PdCo_{0.28}/MgAl-LDH (a₂) and 0.79-PdCo_{0.54}/MgAl-LDH (a₃).

Fig. 5 shows HRTEM images of the catalysts x -PdCo_{0.28}/CoAl-LDH ($x = 0.67, 0.10$ or 0.01 wt%) and 0.64-PdCo_{0.28}/NiAl-LDH. Clearly, the average size of PdCo_{0.28} NCs in 0.67-PdCo_{0.28}/CoAl-LDH is 2.3 ± 0.6 nm (Fig. 5a), which is almost equal to that of 0.86-PdCo_{0.28}/MgAl-LDH, but slightly smaller than that of 0.64-PdCo_{0.28}/NiAl-LDH (2.5 ± 0.6 nm, Fig. 5d). Meanwhile, the PdCo_{0.28} NCs in 0.67-PdCo_{0.28}/CoAl-LDH are prominently dispersed on the edge sites of CoAl-LDH nanosheets as flower-like structures, and this edge effect is seemingly more obvious in the x -PdCo_{0.28}/CoAl-LDH catalysts than in the 0.86-PdCo_{0.28}/MgAl-LDH and 0.64-PdCo_{0.28}/NiAl-LDH catalysts, suggesting the existence of a possibly stronger interaction between PdCo_{0.28} NCs and CoAl-LDH nanoplates. Upon reducing Pd loadings, both 0.10-PdCo_{0.28}/CoAl-LDH (Fig. 5b) and 0.01-PdCo_{0.28}/CoAl-LDH (Fig. 5c), show greatly decreased NC sizes of 1.8 ± 0.5 and 1.6 ± 0.4 nm, respectively. The corresponding high-magnified HRTEM images (Fig. 5a'–d') show the lattice fringes with spacings of 0.220 nm corresponding to the PdCo_{0.28} alloy NC (111) planes, and the lattice fringes with spacings of 0.197 nm corresponding to the hexagonal LDH (018) plane. It is noteworthy that the lowest Pd loading sample 0.01-PdCo_{0.28}/CoAl-LDH shows the smallest size of PdCo_{0.28} NCs, which is approximately equal to that of pure PdCo_{0.28} colloidal NCs (~ 1.5 nm). The above results show that the sizes of PdCo alloy NCs can be significantly tuned by both Co/Pd ratios and Pd loadings, and all the PdCo NCs are mainly dispersed on the edge of isolated LDH nanoplates in the form of flower-like morphologies, implying the strong interaction between PdCo NCs and LDH support; especially the x -PdCo_{0.28}/CoAl-LDH system may show an even stronger interaction between PdCo_{0.28} NCs and CoAl-LDH, which plays a crucial role in catalytic reaction. Additionally, the flower-like structures of the catalysts promote the rapid transportation and diffusion of reactant molecules and expose more accessible active sites, which is beneficial for catalytic activity.

The catalytic performances of the Heck reaction between iodobenzene (PhI) and styrene over the flower-like PdCo alloy NCs catalysts x -PdCo_{*r*}/Co(Mg or Ni)Al-LDH ($r = 0.10, 0.28$ and 0.54 ; $x = 0.01$ – 0.86 wt%) and their related samples are listed in Table 1. The Pd/MgAl-LDH shows a PhI conversion of 38.0% (Table 1, entry 1), while the Co/MgAl-LDH (Table 1, entry 2)

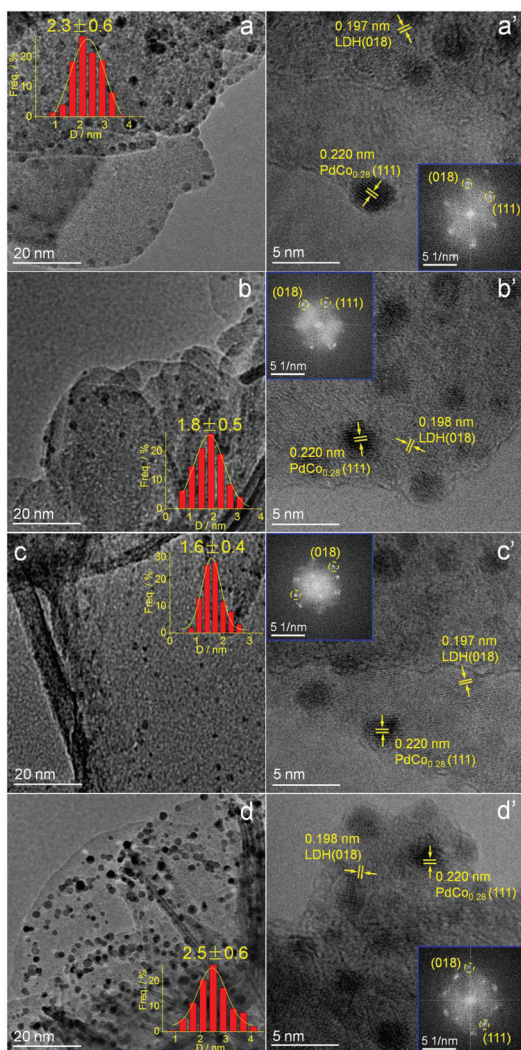


Fig. 5 HRTEM images of 0.67-PdCo_{0.28}/CoAl-LDH (a and a'), 0.10-PdCo_{0.28}/CoAl-LDH (b and b'), 0.01-PdCo_{0.28}/CoAl-LDH (c and c') and 0.64-PdCo_{0.28}/NiAl-LDH (d and d') (insets: particle size distribution and FFT).

shows no activity after 12 h, indicating that metal Pd is an active species for the Heck reaction, which is consistent with the previous report.² After alloying with Co, the catalysts 0.81-PdCo_{0.10}/MgAl-LDH, 0.86-PdCo_{0.28}/MgAl-LDH and 0.79-PdCo_{0.54}/MgAl-LDH (Table 1, entries 3–5) exhibit a much higher activity with 1.67, 2.33 and 1.60 times the turnover frequency (TOF) of Pd/MgAl-LDH, respectively, of which the 0.86-PdCo_{0.28}/MgAl-LDH with a middle Co/Pd ratio shows the highest activity, indicating that the incorporation of Co can significantly improve the Heck reactivity. Upon altering LDH compositions, the 0.67-PdCo_{0.28}/CoAl-LDH (Table 1, entry 7) exhibits the TOF of 661 h⁻¹, which is higher than the 0.86-PdCo_{0.28}/MgAl-LDH (589 h⁻¹) and 0.64-PdCo_{0.28}/NiAl-LDH (537 h⁻¹, Table 1, entry 6), probably due to the combinational effect of ultrafine PdCo_{0.28} NCs and strong interaction between PdCo_{0.28} NCs and CoAl-LDH. Upon reducing Pd loadings, both 0.10-PdCo_{0.28}/CoAl-LDH and 0.01-PdCo_{0.28}/CoAl-LDH (Table 1,

entries 8 and 9) display a remarkably increased TOF of 2405 h⁻¹ and 3317 h⁻¹, respectively. Specifically, the 0.01-PdCo_{0.28}/CoAl-LDH exhibits an extra high TOF of 163 000 h⁻¹ at the Pd usage of 1.9×10^{-5} mol% (Table 1, entry 10), which can be ascribed to the shift of the homeopathic Pd catalysts to the catalytic cycle at a lower Pd dosage.^{35,36} This activity is far higher than that of the currently reported bimetallic hierarchical PdNi-Ni(OH)₂¹⁷ (147 959 h⁻¹, Table 1, entry 11), (RS)₁Au (SL)₀(SL-PdCl₂)_{1.2} with the Pd-complex immobilized on the surface of Au NPs³⁷ (48 700 h⁻¹, Table 1, entry 12) and monometallic Si nanowire array-stabilized Pd NPs (40 000 h⁻¹, Table 1, entry 13),³⁸ and even higher than that of the hierarchical nanosheet array-like catalyst Pd_{0.0098}/CoAl-LDH/rGO at 20 °C higher temperature (160 000 h⁻¹, Table 1, entry 14).³⁹ The above results strongly suggest that the present flower-like PdCo alloy NC catalysts possess excellent activity for the Heck reaction, especially the 0.01-PdCo_{0.28}/CoAl-LDH with the smallest PdCo NCs of ~1.6 nm shows the highest activity, which is probably related to its smallest PdCo_{0.28} alloy NCs and the strong interaction between PdCo_{0.28} alloy NCs and CoAl-LDH.

Moreover, the substrates' adaptability for the Heck reaction of various aryl halides with olefins over 0.01-PdCo_{0.28}/CoAl-LDH is shown (Table 2). Obviously, the catalyst shows excellent catalytic activity for the Heck reaction of styrene and aryl iodides with electron-rich or electron-poor substituents (Table 2, entries 1–5) in an order of TOF values as IPh-NO₂ (10 000 h⁻¹) > IPh-COCH₃ (9100 h⁻¹) > IPh-H (3317 h⁻¹) > IPh-CH₃ (3170 h⁻¹) > IPh-OCH₃ (3083 h⁻¹), which is consistent with the order of the nucleophilicity of the aromatic ring.¹⁴ Additionally, the Heck reaction of PhI with ethyl acrylate or butyl acrylate (Table 2, entries 6 and 7) can be catalyzed efficiently with a TOF of 3260 or 3301 h⁻¹, respectively. Meanwhile, the high activities for the Heck reaction of bromobenzene with styrene or ethyl acrylate are obtained with a TOF of 927 or 1167 h⁻¹, respectively (Table 2, entries 8 and 9), which is much higher than that of the currently reported Pd@Co/CNT-50 (CNT = carbon nanotube, 163 h⁻¹)⁴⁰ and Pd (2.5)/NT (NT = hydrogen titanate nanotubes, 43.2 h⁻¹).⁴¹ It also shows some activity for the Heck reaction of the inactive chlorobenzene with styrene with a TOF of 323 h⁻¹ (Table 2, entry 10). These results suggest that the present flower-like PdCo alloy NC catalysts possess excellent adaptability for substrates.

Furthermore, the recyclability of 0.67-PdCo_{0.28}/CoAl-LDH was carried out. After the reaction, the catalyst was recovered by centrifugation, washed with ethyl acetate and H₂O alternately, and dried at 60 °C for the next run under the same conditions. The recovered sample shows a PhI conversion of 94.7% and a *trans*-stilbene selectivity of 98.0% (Fig. S5A†) after 12 runs. The SEM (Fig. S5B†) and HRTEM images (Fig. S5C and D†) of the recovered catalyst clearly show the well-kept nanosheets' flower-like structure. The average size of the PdCo_{0.28} alloy NCs of 2.4 ± 0.9 nm is almost the same as the fresh one (2.3 ± 0.6 nm) with the PdCo_{0.28} NCs predominantly dispersed on the edge sites of the CoAl-LDH nanosheets. The lattice fringes with spacings of 0.220 and 0.197 nm indexed to the PdCo_{0.28} alloy NCs (111) plane and hexagonal LDH (018)

Table 1 Catalytic activities of various catalysts for Heck reaction^a

Entry	Catalysts	Pd/mol%	t/h	Conv./%	Yield/%	TOF ^b /h ⁻¹	Ref.
1	Pd/MgAl-LDH	0.30	0.5/1.3	38.0/96.0	37.2/94.0	253/246	This
2	Co/MgAl-LDH	0.30	0.5/12	n.d.	n.d.	n.d.	This
3	0.81-PdCo _{0.10} /MgAl-LDH	0.30	0.5/1.2	63.4/99.7	61.8/98.4	423/277	This
4	0.86-PdCo _{0.28} /MgAl-LDH	0.30	0.5/1	88.3/99.6	86.6/97.2	589/332	This
5	0.79-PdCo _{0.54} /MgAl-LDH	0.30	0.5/1.2	60.6/99.1	59.4/96.6	404/275	This
6	0.64-PdCo _{0.28} /NiAl-LDH	0.30	0.5	80.6	76.3	537	This
7	0.67-PdCo _{0.28} /CoAl-LDH	0.30	0.5	99.1	96.2	661	This
8	0.10-PdCo _{0.28} /CoAl-LDH	0.02	2	68.8	68.0	1720	This
9	0.01-PdCo _{0.28} /CoAl-LDH	0.02	2	96.2	93.2	2405	This
10	0.01-PdCo _{0.28} /CoAl-LDH ^c	1.9 × 10 ⁻⁵	3	93	9.0	163 000	This
11	Hierarchical PdNi-Ni(OH) ₂ ^d	2.45 × 10 ⁻⁵	24	—	87	147 959	17
12	(RS) ₁ Au(SL) ₆ (SL-PdCl ₂) _{1.2} ^e	1.0 × 10 ⁻⁵	2	—	97.3	48 700	37
13	Si nanowire array-stabilized Pd NPs ^f	4.9 × 10 ⁻⁵	48	—	95	40 000	38
14	Hierarchical nanosheet array-like Pd _{0.0098} /CoAl-LDH/rGO ^g	1.0 × 10 ⁻⁴	1	16	—	160 000	39

^a Reaction conditions: PhI (1 mmol), styrene (1.5 mmol), $\nu_{\text{DMF}}:\nu_{\text{H}_2\text{O}} = 12 \text{ mL} : 4 \text{ mL}$, K_2CO_3 (3 mmol), 120 °C under atmospheric conditions.

^b Turnover frequency (TOF): the converted moles of PhI per mole of Pd per hour. ^c Reaction conditions: PhI (50 mmol), styrene (75 mmol), $\nu_{\text{DMF}}:\nu_{\text{H}_2\text{O}} = 120 \text{ mL} : 40 \text{ mL}$, K_2CO_3 (100 mmol), 120 °C under atmospheric conditions. ^d Reaction conditions: PhI (50 mmol), butyl acrylate (100 mmol), Et_3N (150 mmol), TBAA (10 mmol), 160 °C. ^e Reaction conditions: PhI (10 mmol), butyl acrylate (10 mmol), Et_3N (1.5 mL), DMSO (1 mL), 115 °C. ^f Reaction conditions: PhI (50 mmol), butyl acrylate (100 mmol), Et_3N (150 mmol), TBAA (10 mmol), 160 °C. ^g Reaction conditions: PhI (50 mmol), styrene (60 mmol), $\nu_{\text{DMF}}:\nu_{\text{H}_2\text{O}} = 120 \text{ mL} : 40 \text{ mL}$, K_2CO_3 (100 mmol), 140 °C under atmospheric conditions.

Table 2 Catalytic activities for the Heck reaction of different aryl halides with various alkenes over 0.01-PdCo_{0.28}/CoAl-LDH^a

Entry	Substrate (1)		Alkene (2) <i>R</i> ₂	<i>t</i> /h	Conv. ^b /%	TOF ^c /h ⁻¹
	X	<i>R</i> ₁				
1	I	NO ₂	Ph	0.5	100 (3a)	10 000
2	I	COCH ₃	Ph	0.5	91.0 (3b)	9100
3	I	H	Ph	1.5	98.1 (3c)	3317
4	I	CH ₃	Ph	1.5	95.1 (3d)	3170
5	I	OCH ₃	Ph	1.5	92.5 (3e)	3083
6	I	H	CO ₂ CH ₃	1.5	97.8 (3f)	3260
7	I	H	CO ₂ C ₄ H ₉	1.5	99.1 (3g)	3301
8	Br	H	Ph	5.0	92.7 (3c)	927
9	Br	H	CO ₂ CH ₃	4.0	93.9 (3f)	1167
10	Cl ^d	H	Ph	10.0	64.6 (3c)	323

^a Reaction conditions: 0.01-PdCo_{0.28}/CoAl-LDH (Pd: 0.02 mol% based on the amount of aryl halide), aryl halide (1.0 mmol), alkene (1.2 mmol), $\nu_{\text{DMF}}:\nu_{\text{H}_2\text{O}} = 12 \text{ mL} : 4 \text{ mL}$, K_2CO_3 (3.0 mmol), 120 °C under atmospheric conditions. ^b Determined By GC, identified by ¹H and ¹³C NMR. ^c Turnover frequency (TOF): the converted moles of PhI (PhBr or PhCl) per mole of Pd per hour. ^d Reaction conditions: 0.01-PdCo_{0.28}/CoAl-LDH (Pd: 0.02 mol%), aryl halide (1.0 mmol), alkene (1.2 mmol), $\nu_{\text{DMF}}:\nu_{\text{H}_2\text{O}} = 12 \text{ mL} : 4 \text{ mL}$, K_2CO_3 (3.0 mmol), 140 °C.

plane (Fig. S5E[†]), respectively, are still observed clearly. The ICP analysis of the supernatant (detection limit: 0.01 ppm) after 12 runs shows no leaching of Pd and Co species. These results clearly suggest that the present PdCo alloy NC catalysts possess excellent structural stability and recyclable efficiency.

In order to get an insight into the nature of the Heck reaction over the flower-like PdCo alloy NC catalysts, the macroscopic kinetics of the catalysts *x*-PdCo_{*y*}/MgAl-LDH has been conducted, including the effect of Co/Pd ratios and reaction

temperatures on Heck reactivity. It can be seen clearly from Fig. S6[†] that the conversion (*C*) of PhI increases linearly up to ~70% with a prolonged time (*t*) over these three catalysts, implying the weak inhibition of the product. As shown in Fig. 6a₁–a₃, the plots of $-\ln(1 - C)$ against *t* for three catalysts show a linear correlation, indicating a first-order reaction characteristic with respect to PhI. The Heck reaction rate constant (*k*) values for three catalysts (Table S2[†]), obtained by calculating the slope of the $-\ln(1 - C)$ versus *t* plots, show a decrease in an order of 0.86-PdCo_{0.28}/MgAl-LDH > 0.81-PdCo_{0.10}/MgAl-LDH > 0.79-PdCo_{0.54}/MgAl-LDH. Meanwhile, the plots of $\ln k$ versus the inverse of absolute temperature

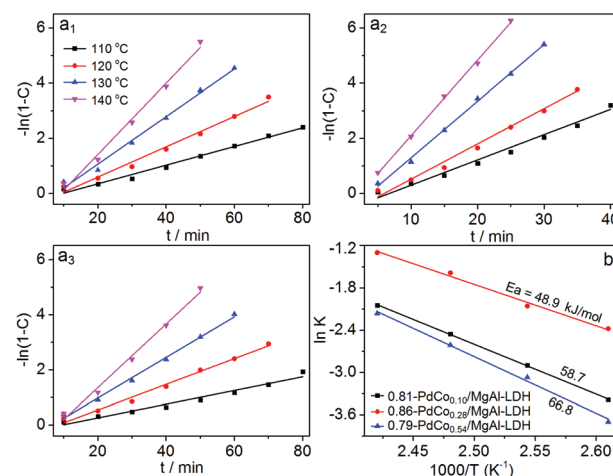


Fig. 6 $-\ln(1 - C)$ against time (a₁–a₃) and Arrhenius plots (b) for the Heck reaction over 0.81-PdCo_{0.10}/MgAl-LDH (a₁), 0.86-PdCo_{0.28}/MgAl-LDH (a₂) and 0.79-PdCo_{0.54}/MgAl-LDH (a₃) at different temperatures. Reaction conditions: catalyst (Pd: 0.3 mol% upon PhI), PhI (1 mmol), styrene (1.5 mmol), $\nu_{\text{DMF}}:\nu_{\text{H}_2\text{O}} = 12 \text{ mL} : 4 \text{ mL}$, K_2CO_3 (3 mmol).

show a good linear relationship (Fig. 6b), and the calculated apparent activation energy (E_a) from the slope with the least-square fit is listed in Table S2.† Clearly, the 0.86-PdCo_{0.28}/MgAl-LDH possesses the smallest E_a value of 48.9 kJ mol⁻¹, which is significantly lower than those of 0.81-PdCo_{0.10}/MgAl-LDH (58.7 kJ mol⁻¹) and 0.79-PdCo_{0.54}/MgAl-LDH (66.8 kJ mol⁻¹). The above results indicate that 0.86-PdCo_{0.28}/MgAl-LDH possesses the highest k and the lowest E_a value among the x -PdCo _{x} /MgAl-LDH catalysts, in line with its highest Heck reactivity.

To explore the relationship between structure and performance on the flower-like PdCo alloy NCs catalysts, XPS and *in situ* CO FT-IR analyses were performed for a series of the PdCo alloy NC catalysts.

The XPS results (Fig. 7) reveal that Pd/MgAl-LDH shows two distinct broad peaks at binding energies (BEs) of ~336.30 and ~340.5 eV, which can be attributed to Pd 3d_{5/2} and Pd 3d_{3/2} core levels,⁴² respectively. The deconvolution BE values of Pd 3d_{5/2} at 335.70 and 337.30 eV can be assigned to Pd⁰ and Pd^{II} species, respectively, and the percentage of Pd⁰ is 78.0%. The Co/MgAl-LDH displays two broad peaks at ~778.80 and ~785.70 eV, which can be attributed to Co 2p_{3/2} and Co 2p_{1/2} core levels,⁴² respectively, indicating the existence of metallic Co⁰ species. After alloying with Co, the catalysts 0.81-PdCo_{0.10}/MgAl-LDH, 0.86-PdCo_{0.28}/MgAl-LDH and 0.79-PdCo_{0.54}/MgAl-

LDH (Fig. 7A(a₁-a₃)) show the Pd⁰ 3d_{5/2} BE values at 335.25, 334.69 and 334.92 eV, respectively, shifting to a low BE with the corresponding offsets of 0.45, 1.01, and 0.78 eV compared with Pd/MgAl-LDH, indicating the increased electron density of the Pd⁰ center.^{15,39,42} The Co 2p_{3/2} BE values of three catalysts (Fig. 7B(a₁-a₃)) at 778.25, 777.80 and 778.15 eV, respectively, with decreases of 0.55, 1.00 and 0.65 eV compared to Co/MgAl-LDH indicate the decreased electron density of Co⁰ species.^{19,42} The negative shift of both Pd 3d_{5/2} and Co 2p_{3/2} clearly demonstrates the electron transfer from Co to Pd atom, especially the 0.86-PdCo_{0.28}/MgAl-LDH shows the most electron-rich Pd species, suggesting its strongest interaction between Pd and Co. Meanwhile, the percentages of Pd⁰ species of 90.9, 100 and 86.0% (Table S3†) for 0.81-PdCo_{0.10}/MgAl-LDH, 0.86-PdCo_{0.28}/MgAl-LDH and 0.79-PdCo_{0.54}/MgAl-LDH, respectively, are higher than that for Pd/MgAl-LDH (78.0%), probably due to the proper Co-doping inhibiting the oxidation of Pd⁰ species especially for the sample 0.86-PdCo_{0.28}/MgAl-LDH.

The O 1s spectra of 0.81-PdCo_{0.10}/MgAl-LDH, 0.86-PdCo_{0.28}/MgAl-LDH and 0.79-PdCo_{0.54}/MgAl-LDH (Fig. S7A(a₁-a₃)†) show that an apparent asymmetric envelope peak in 527-537 eV can be fitted into three peaks, which can be attributed to the surface lattice O²⁻ (530-531 eV), OH (531-532 eV) and the adsorbed or interlayer H₂O (532-534 eV),⁴² respectively. The surface OH content in the three catalysts decreases to 68.1%-69.2% compared with MgAl-LDH (73.3%, Table S3†), suggesting the existence of a strong interaction between PdCo NCs and the surface OH groups of LDH. Particularly, the 0.86-PdCo_{0.28}/MgAl-LDH with the largest surface OH content of 69.2% possesses the strongest PdCo_{0.28} NCs - MgAl-LDH interaction. Meanwhile, the Mg 2p BE values (Fig. S7B(a₁-a₃)†) are 50.16, 50.19 and 50.14 eV for 0.81-PdCo_{0.10}/MgAl-LDH, 0.86-PdCo_{0.28}/MgAl-LDH, and 0.79-PdCo_{0.54}/MgAl-LDH, respectively, which are slightly higher than those of Pd/MgAl-LDH (50.05 eV) and Co/MgAl-LDH (50.09 eV), and all these values are slightly shifted toward high BE values compared with MgAl-LDH (50.01 eV), suggesting the existence of a proper interaction between PdCo NCs and MgAl-LDH. Specifically, the 0.86-PdCo_{0.28}/MgAl-LDH with the largest offset (0.18 eV) exhibits the strongest PdCo_{0.28} NCs - MgAl-LDH synergistic interaction, which is consistent with Pd 3d and Co 2p XPS data.

The above results show that the incorporation of Co not only provides electrons to Pd⁰ species, but also inhibits the oxidation of Pd⁰ species, of which 0.86-PdCo_{0.28}/MgAl-LDH with a Co/Pd ratio of 0.28 possesses the highest electron density of the Pd⁰ centre and the largest content of Pd⁰ species and the strongest PdCo_{0.28} NCs - MgAl-LDH interaction, in line with its highest Heck reactivity.

Furthermore, the Pd 3d XPS spectra of the 0.67-PdCo_{0.28}/CoAl-LDH with an even higher activity (Fig. 7A(b₁)) clearly show two distinct peaks assigned to Pd⁰ 3d_{5/2} (334.50 eV) and 3d_{3/2} (339.80 eV), and the Pd⁰ 3d_{5/2} peak shifts to a low BE with an offset of 0.50 eV compared with bulk Pd (335.00 eV), indicating the increased electron density of the Pd⁰ centre of the catalyst.^{15,39} In contrast, Co 2p XPS (Fig. 7B(b₁)) fails to show the peaks for the Co⁰ species from the PdCo_{0.28} NCs

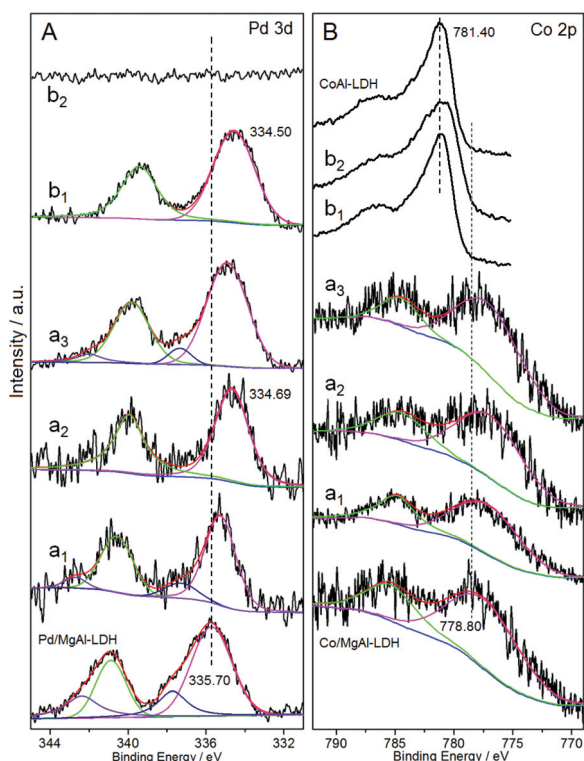


Fig. 7 Pd 3d (A) and Co 2p (B) XPS spectra of 0.81-PdCo_{0.10}/MgAl-LDH (a₁), 0.86-PdCo_{0.28}/MgAl-LDH (a₂), 0.79-PdCo_{0.54}/MgAl-LDH (a₃), compared with monometallic Pd/MgAl-LDH and Co/MgAl-LDH; and 0.67-PdCo_{0.28}/CoAl-LDH (b₁), and 0.01-PdCo_{0.28}/CoAl-LDH (b₂) compared with CoAl-LDH support.

probably due to the overlapping of a strong signal originating from $\text{Co}^{2+} 2p_{3/2}$ from the CoAl-LDH as the peaks at ~ 780.80 ($\text{Co}^{2+} 2p_{3/2}$) indicated. The higher offset for $\text{Pd}^0 3d_{5/2}$ BE compared with the bulk Pd in 0.67-PdCo_{0.28}/CoAl-LDH than in 0.86-PdCo_{0.28}/MgAl-LDH (0.31 eV) is reasonable for the higher activity of the former. The lower surface OH content (Table S3†) of 75.5% than CoAl-LDH (78.3%) indicates the existence of a strong PdCo NCs – CoAl-LDH interaction, in line with the Pd 3d and Co 2p XPS results. Meanwhile, the XPS data of the recovered samples of 0.67-PdCo_{0.28}/CoAl-LDH after 4, 8 and 12 runs (Fig. S5F†) also reveal the microstructure stability of the catalyst during the catalytic process (details are in the ESI†).

Then for 0.01-PdCo_{0.28}/CoAl-LDH with the highest activity, the Pd 3d signal (Fig. 7A(b₂)) cannot be observed probably due to its ultralow Pd loading of 0.01 wt%, and the Co 2p XPS only shows the peaks of the Co^{2+} species from support, contrarily confirming the ultrahigh dispersion of the PdCo NCs in this catalyst. It should be noted that the $\text{Co}^{2+} 2p_{3/2}$ BE value shows a larger downshift of 0.80 eV compared to CoAl-LDH, than 0.67-PdCo_{0.28}/CoAl-LDH (0.60 eV), indicating more electron transfer from the Co^{2+} -OH group of the support to PdCo NCs, and indirectly implying a stronger PdCo_{0.28} NCs – CoAl-LDH synergistic interaction in 0.01-PdCo_{0.28}/CoAl-LDH with a slightly higher surface OH content (76.1%, Table S3†), in line with its highest Heck coupling activity.

Fig. 8 shows the CO *in situ* FTIR spectra of the catalysts 0.81-PdCo_{0.10}/MgAl-LDH, 0.86-PdCo_{0.28}/MgAl-LDH and 0.79-PdCo_{0.54}/MgAl-LDH compared with the monometallic samples. For all the samples, a distinctly strong peak at 2170 cm^{-1} which is commonly observed can be attributed to the stretching frequency of CO adsorbed on Brønsted acid sites related to the $\text{AlO-H}^{\delta+}$ centre on LDH in a linear mode.^{43,44} A sharp strong peak at 1914 cm^{-1} and a weak one at

2040 cm^{-1} for Pd/MgAl-LDH can be attributed to the CO molecule adsorbed on the Pd atom in the bridge mode and linear mode,⁴⁵ respectively, while a broad peak at 2052 cm^{-1} for Co/MgAl-LDH is due to the CO molecule adsorbed on the metallic Co sites in a linear mode.⁴⁶ For three bimetallic catalysts (Fig. 8a₁–a₃), the intensity of the peak at ~ 1914 cm^{-1} gradually weakens with increasing Co/Pd ratios, indicating that more and more CO molecules are adsorbed on Pd sites in a linear mode (~ 2033 cm^{-1}). Meanwhile, the peak areas of CO linearly adsorbed on Pd atoms in these three catalysts account for 83.1, 95.4 and 98.2% of the total area of linear and bridged CO peaks, respectively, which is significantly higher than that of Pd/MgAl-LDH (60.5%), suggesting that surface continuous Pd sites can be isolated by the doped Co atoms. In detail, the linear CO adsorbed peaks of Pd atoms in the three catalysts are located at 2033, 2024 and 2035 cm^{-1} , respectively, showing a remarkable redshift compared with Pd/MgAl-LDH (2040 cm^{-1}). Particularly, the 0.86-PdCo_{0.28}/MgAl-LDH shows the largest redshift of 16 cm^{-1} , indicating the highest electron density of Pd^0 species, in line with XPS results. The aforementioned results indicate that the incorporation of Co significantly isolates the surface continuous Pd sites and the adjacent Co atoms modify the electronic structure of the active Pd species in the obtained PdCo alloy NC catalysts. Specifically, 0.86-PdCo_{0.28}/MgAl-LDH exhibits the highest electron density of the Pd^0 centre in the three x -PdCo _{y} /MgAl-LDH catalysts, which is consistent with its highest Heck reactivity.

In order to confirm whether the catalytic mechanism of the present catalysts follows a homogeneous or heterogeneous catalytic reaction path, hot filtration experiments have been conducted.¹⁴ Two parallel tests have been carried out over 0.67-PdCo_{0.28}/CoAl-LDH (0.3 mol%). The first one is proceeded until the completion of the reaction (99.2%, 35 min), and the plot of PhI conversion *versus* reaction time is shown curves a in Fig. S8.† For the second test (curves b, Fig. S8†), the catalyst was separated from the reaction mixture at a PhI conversion of 56.3% by hot filtration. The ICP analysis of the filtrate shows only 0.02 ppm Pd (corresponding to 1.5 wt% of the total amount of Pd) leached. The filtrate was allowed to continue reacting for another 1.2 h under the same conditions, and the PhI conversion remained almost unchanged. These results suggest that only the Pd species from PdCo NCs bound to CoAl-LDH can catalyze the Heck reaction, that is, the reaction occurs on the surface of the present catalysts.

Based on the above experiments and XPS as well as CO *in situ* FTIR analyses combined with previous findings about the generally accepted mechanism,^{47–50} a possible Heck coupling mechanism on the present flower-like PdCo alloy NC catalysts (Scheme 2) was tentatively proposed. First, the oxidative addition of PdCo alloy NCs with aryl halides is formed to surface organometallic intermediates.⁴⁹ It is noteworthy that both Co atoms adjacent to the Pd atoms and surface –OH groups of the flower-like LDH support contributed to the increased electron density of the Pd center to promote the oxidative addition of the aryl halides in this step. Meanwhile, the flower-like structure of the present catalysts also contributed to

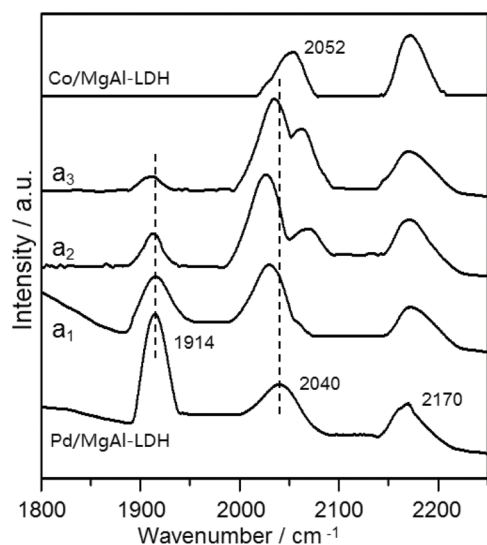
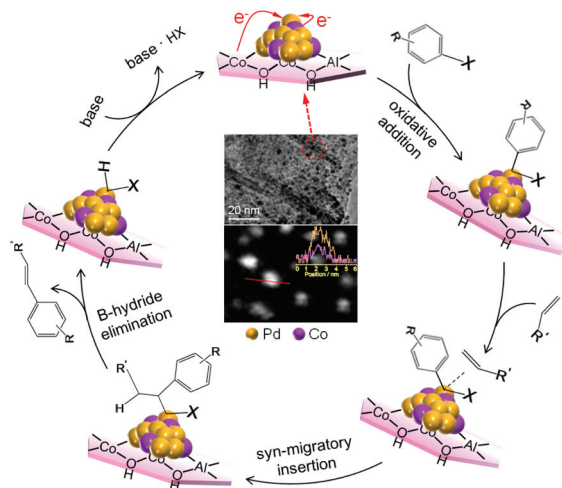


Fig. 8 CO FTIR spectra of 0.81-PdCo_{0.10}/MgAl-LDH (a₁), 0.86-PdCo_{0.28}/MgAl-LDH (a₂), 0.79-PdCo_{0.54}/MgAl-LDH (a₃) compared with the monometallic Pd/MgAl-LDH and Co/MgAl-LDH.



Scheme 2 Plausible mechanism of Heck coupling of aryl halides with alkenes over the x -PdCo_{0.28}/Co(Mg or Ni)Al-LDH catalysts.

this oxidative addition *via* promoting the rapid transportation and diffusion of the substrate molecules, in favor of efficient collision with active sites. Second, olefin and surface organometallic intermediates are coordinated followed by its synmigratory insertion which is intimately related to the size of the active PdCo, alloy NCs and PdCo NCs – LDH synergistic interaction. Third, the newly generated organometallic species undergoes *syn* β -hydrogen elimination to form olefinic compounds. Lastly, the base promotes the elimination of H-X to regenerate the Pd⁰ catalysts, wherein the intrinsic alkalinity of the LDH may promote this elimination to regenerate the catalyst to some extent.

Conclusion

A series of nanosheet flower-like PdCo alloy nanocluster (NC) catalysts x -PdCo_{0.28}/Co(Mg or Ni)Al-LDH were fabricated *via* a sol immobilization strategy. The sizes of PdCo alloy NCs can be effectively tuned within ~1.6–3.2 nm by both Co/Pd ratios and Pd loadings in the as-obtained catalysts, and the PdCo NCs are mainly dispersed on the edge sites of the LDH nanosheets with a flower-like morphology. The 0.81-PdCo_{0.10}/MgAl-LDH, 0.86-PdCo_{0.28}/MgAl-LDH and 0.79-PdCo_{0.54}/MgAl-LDH catalysts exhibit better iodobenzene – styrene Heck activity than Pd/MgAl-LDH. Particularly, 0.86-PdCo_{0.28}/MgAl-LDH shows the highest TOF value, which can be attributed to its smallest PdCo_{0.28} alloy NCs, and the maximum electron density of the Pd centre (the maximum content of Pd⁰ species) originated from electron transfer from Co and the strongest PdCo_{0.28} NCs–LDH synergistic interaction. The 0.67-PdCo_{0.28}/CoAl-LDH catalyst shows a much higher TOF than those of the 0.64-PdCo_{0.28}/NiAl-LDH and 0.86-PdCo_{0.28}/MgAl-LDH catalysts. The lowest Pd loading sample 0.01-PdCo_{0.28}/CoAl-LDH (~1.6 nm) shows an ultrahigh TOF of 163 000 h⁻¹ at the Pd dosage of 1.9×10^{-5} mol%, which can be attributed to its smallest PdCo_{0.28}

alloy NCs and strongest PdCo_{0.28} NCs–CoAl-LDH synergistic interaction. Meanwhile, the catalyst possesses excellent substrate universality for the Heck reaction and can be reused for 12 runs without significant loss of activity. The current work may provide a new idea for the simple and green synthesis of ultrafine Pd-based low-cost non-noble bimetallic catalysts for various catalytic processes.

Conflicts of interest

There are no conflicts to declare.

Acknowledgements

This work was supported by the National Natural Science Foundation of China (21878007, 21576013 and 21521005).

References

- 1 J. Choi and G. C. Fu, *Science*, 2017, **356**, 1–8.
- 2 A. Biffis, P. Centomo, A. D. Zotto and M. Zecca, *Chem. Rev.*, 2018, **118**, 2249–2295.
- 3 B. M. Trost, J. D. Knopf and C. S. Brindle, *Chem. Rev.*, 2016, **116**, 15035–15088.
- 4 J. Magano and J. R. Dunetz, *Chem. Rev.*, 2011, **111**, 2177–2250.
- 5 C. Torborg and M. Beller, *Adv. Synth. Catal.*, 2009, **351**, 3027–3043.
- 6 Z. Feng, Q. Q. Min, H. Y. Zhao, J. W. Gu and X. G. Zhang, *Angew. Chem., Int. Ed.*, 2015, **54**, 1270–1274.
- 7 A. Qrtiz, P. Gómez-Sal, J. C. Flores and E. Jesús, *Organometallics*, 2018, **37**, 3598–3610.
- 8 A. Bruneau, M. Roche, M. Alami and S. Messaoudi, *ACS Catal.*, 2015, **5**, 1386–1396.
- 9 P. W. Liu, Z. M. Dong, Z. B. Ye, W. J. Wang and B. G. Li, *J. Mater. Chem. A*, 2013, **1**, 15469–15478.
- 10 E. Fernández, M. A. Rivero-Crespo, I. Domínguez, P. Rubio-Marqués, J. Oliver-Meseguer, L. C. Liu, M. Cabrero-Antonino, R. Gavara, J. C. Hernández-Garrido, M. Boronat, A. Leyva-Pérez and A. Corma, *J. Am. Chem. Soc.*, 2019, **141**, 1928–1940.
- 11 P. Y. Wang, G. H. Zhang, H. Y. Jiao, L. W. Liu, X. Y. Deng, Y. Chen and X. P. Zheng, *Appl. Catal., A*, 2015, **489**, 188–192.
- 12 Y. Wan, H. Y. Wang, Q. F. Zhao, M. Klingstedt, Q. Terasaki and D. Y. Zhao, *J. Am. Chem. Soc.*, 2009, **131**, 4541–4550.
- 13 A. K. Rathi, M. B. Gawande, J. Pechousek, J. Tucek, C. Aparicio, M. Petr, O. Tomanec, R. Krikavova, Z. Travnicek, R. S. Varma and R. Zboril, *Green Chem.*, 2016, **18**, 2363–2373.
- 14 B. M. Choudary, S. Madhi, N. S. Chowdari, M. L. Kantam and B. Sreedhar, *J. Am. Chem. Soc.*, 2002, **124**, 14127–14136.
- 15 P. Li, P.-P. Huang, F.-F. Wei, Y.-B. Sun, C.-Y. Cao and W.-G. Song, *J. Mater. Chem. A*, 2014, **2**, 12739–12745.

- 16 G. Y. Bao, J. Bai and C. P. Li, *Org. Chem. Front.*, 2019, **6**, 352–261.
- 17 H. Fan, X. Huang, L. Shang, Y. T. Cao, Y. F. Zhao, L.-Z. Wu, C.-H. Tung, Y. D. Yin and T. R. Zhang, *Angew. Chem., Int. Ed.*, 2016, **55**, 2167–2170.
- 18 S. Diyarbakir, H. Can and Ö. Metin, *ACS Appl. Mater. Interfaces*, 2015, **7**, 3199–3206.
- 19 A. Shaabani and M. Mahyari, *J. Mater. Chem. A*, 2013, **1**, 9303–9311.
- 20 L.-X. You, H.-J. Liu, L.-X. Cui, F. Ding, G. Xiong, S.-J. Wang, B.-Y. Ren, I. Dragutan, V. Dragutan and Y.-G. Sun, *Dalton Trans.*, 2016, **45**, 18455–18458.
- 21 M. Dabiri and M. P. Vajargahy, *Appl. Organomet. Chem.*, 2017, **31**, e3594.
- 22 G. L. Fan, F. Li, D. G. Evans and X. Duan, *Chem. Soc. Rev.*, 2014, **43**, 7040–7066.
- 23 Z. T. Wang, Y. J. Song, J. H. Zou, L. Y. Li, Y. Yu and L. Wu, *Catal. Sci. Technol.*, 2018, **8**, 268–275.
- 24 Y. Y. Du, Q. Jin, J. T. Feng, N. Zhang, Y. F. He and D. Q. Li, *Catal. Sci. Technol.*, 2015, **5**, 3216–3225.
- 25 L. Li, L. G. Dou and H. Zhang, *Nanoscale*, 2015, **6**, 3753–3763.
- 26 W. G. Menezes, L. Altmann, V. Zielasek, K. Thiel and M. Bäumer, *J. Catal.*, 2013, **300**, 125–135.
- 27 A. R. Denton and N. W. Ashcroft, *Phys. Rev. A: At., Mol., Opt. Phys.*, 1991, **43**, 3161–3164.
- 28 Y.-S. Feng, X.-Y. Lin, J. Hao and H.-J. Xu, *Tetrahedron*, 2014, **70**, 5249–5253.
- 29 Z. Y. Zhang, S. S. Liu, X. Tian, J. Wang, P. Xu, F. Xiao and S. Wang, *J. Mater. Chem. A*, 2017, **5**, 10876–10884.
- 30 S. Maheswari, S. Karthikeyan, P. Murugan, P. Sridhar and S. Pitchumani, *Phys. Chem. Chem. Phys.*, 2012, **14**, 9683–9695.
- 31 P. S. Braterman, Z. P. Xu and F. Yarberry, *Handbook of layered materials*, Wiley, New York, 2004.
- 32 K. Nakamoto, in *Handbook of Vibrational Spectroscopy*, ed. J. M. Chalmers and P. R. Griffiths, John Wiley & Sons, Ltd., New York, 2006, vol. 3.
- 33 J. Y. Liu, *ChemCatChem*, 2011, **3**, 934–948.
- 34 M. Cargnello, V. V. T. Doan-Nguyen, T. R. Gordon, R. E. Diaz, E. A. Stach, R. J. Gorte, P. Fornasiero and C. B. Murray, *Science*, 2013, **341**, 771–773.
- 35 A. H. M. de Vries, J. M. C. A. Mulders, J. H. M. Mommers, H. J. W. Henderickx and J. G. de Vries, *Org. Lett.*, 2003, **5**, 3285–3288.
- 36 C. Deraedt and D. Astruc, *Acc. Chem. Res.*, 2014, **47**, 494–503.
- 37 J.-N. Young, T.-C. Chang, S.-C. Tsai, L. Yang and S. J. Yu, *J. Catal.*, 2010, **272**, 253–261.
- 38 Y. M. A. Yamada, Y. Yuyama, T. Sato, S. Fujikawa and Y. A. Uozumi, *Angew. Chem., Int. Ed.*, 2014, **53**, 127–131.
- 39 Y. N. Wang, L. G. Dou and H. Zhang, *ACS Appl. Mater. Interfaces*, 2017, **9**, 38784–38795.
- 40 A. Zhou, R.-M. Guo, J. Zhou, Y. B. Dou, Y. Chen and J.-R. Li, *ACS Sustainable Chem. Eng.*, 2018, **6**, 2103–2111.
- 41 M. E. Martínez-Klimov, P. Hernandez-Hipólito, T. E. Klimova, D. A. Solís-Casados and M. Martínez-García, *J. Catal.*, 2016, **342**, 138–150.
- 42 J. F. Moulder, W. F. Stickel, P. E. Sobol and K. D. Bomben, in *Handbook of X-ray Photoelectron Spectroscopy*, ed. J. Chastain, Perkin-Elmer Co., Minnesota, 1992.
- 43 W. H. Fang, J. S. Chen, Q. H. Zhang, W. P. Deng and Y. Wang, *Chem. – Eur. J.*, 2011, **17**, 1247–1256.
- 44 M. J. Climent, A. Corma, P. D. Frutos, S. Iborra, M. Noy, A. Velty and P. Concepción, *J. Catal.*, 2010, **269**, 140–149.
- 45 M. S. Chen, D. Kumar, C.-W. Yi and D. W. Goodman, *Science*, 2005, **310**, 291–293.
- 46 T. Montanari, O. Marie, M. Daturi and G. Busca, *Appl. Catal., B*, 2007, **71**, 216–222.
- 47 R. F. Heck and J. P. Nolley, *J. Org. Chem.*, 1972, **37**, 2320–2322.
- 48 N. Yuan, V. Pascanu, Z. H. Huang, A. Valiente, N. Heidenreich, S. Leubner, A. K. Inge, J. Gaar, N. Stock, I. Persson, B. Martín-Matute and X. D. Zou, *J. Am. Chem. Soc.*, 2018, **140**, 8206–8217.
- 49 J. Li, Y. J. Wang, S. W. Jiang and H. Zhang, *J. Organomet. Chem.*, 2018, **878**, 84–95.
- 50 C. C. C. Johansson Seechurn, M. O. Kitching, T. J. Colacot and V. Snieckus, *Angew. Chem., Int. Ed.*, 2012, **51**, 5062–5085.